PHYSICAL REVIEW D **93,** 064075 (2016)

Relativistic tidal effects in nonstandard Kerr spacetime

Andrea Maselli,[1,*] Kostas Kokkotas,[1,2,†] and Pablo Laguna[2,‡]

[1]*Theoretical Astrophysics, Eberhard Karls University of Tuebingen, Tuebingen 72076, Germany*
[2]*Center for Relativistic Astrophysics and School of Physics, Georgia Institute of Technology, Atlanta, Georgia 30332, USA*

(Received 4 February 2016; published 29 March 2016)

Astrophysical phenomena involving massive black holes (BHs) in close binaries are expected to leave detectable signatures in the electromagnetic and gravitational-wave spectrum. Such imprints may provide precious information to probe the space-time around rotating BHs and to reveal new insights on the nature of gravity in the strong-field regime. To support this observational window, it is crucial to develop suitable tests to verify the predictions of General Relativity. In this framework, the metric recently proposed by Johannsen and Psaltis parametrizes strong-field deviations from a Kerr space-time in a theory-independent way. In the following, we make use of this approach to describe the tidal field produced by spinning BHs. We compute the gravito-magnetic and gravito-electric tidal tensors for particles moving on equatorial circular geodesics, comparing our results with those obtained in the standard General Relativity scenario. Our calculations show significant differences even for distances far form the last stable orbit, which may affect the evolution of the binary and leave detectable signatures. We test our framework computing quasiequilibrium sequences of BH-white dwarf systems by means of the affine model, for different binary configurations.

DOI: 10.1103/PhysRevD.93.064075

I. INTRODUCTION

Since its formulation 100 years ago, General Relativity (GR) has successfully passed a large set of observational and experimental tests [1]. Most of them, however, probed only the weak field regime of gravity, and therefore a number of strong-field GR predictions still remain to be verified [2–5]. Black holes are among the most genuine of such predictions, with no analog in the Newtonian theory, and represent the ideal candidates to test gravity under extreme conditions. In General Relativity, black holes (BHs) belong to the Kerr family, and according to the no-hair theorem, their exterior stationary and isolated gravitational field depend only on two parameters: their mass and angular momentum [6]. Initial deviations from the Kerr metric are rapidly radiated away by the emission of gravitational radiation [7]. A proof of the validity of the no-hair theorem is still lacking. However, future electromagnetic [8–11] and gravitational-wave [12,13] observations promise to shed new light on this scenario and are expected to prove the *Kerr hypothesis*. In this regard, several efforts have been devoted to develop independent tests to determine the features of the strong gravitational field in the BH surroundings. Such tests follow a bottom-up approach, in which the BH space-time is parametrized in a phenomenological way, with the aim to map possible detected deviations in terms of an alternative theory of gravity. Requiring that the new metric is free of pathologies as naked singularities or closed timelike curves makes these studies an extremely difficult task. We refer the reader to Ref. [14] and references therein, for a systematic study of the main features of some parametric frameworks which have been proposed in the literature.

In this work, we make use of the new approach recently developed by Johannsen and Psaltis (JP) [15]. The authors introduced polynomial corrections into the Schwarzschild metric as initial seeds, showing that this ansatz can be turned into a Kerr-like metric through the Newmam-Janis algorithm [16]. The mathematical properties and the topology of the JP metric as well as their astrophysical implications have been extensively studied in Refs. [14,15,15,17–19]. Moreover, tests involving properties of iron lines, quasiperiodic oscillations, continuum spectra of accretion disks and images of the accretion flows have been analyzed in Refs. [20–25]. This metric has been also extended to a more general parametrization in Ref. [26], where the authors addressed some unexplored key features of the original framework.

In this paper, we investigate the effects of strong-gravity corrections captured by the JP approach, on the tidal field produced by rotating BHs. We derive the expressions for the gravito-magnetic and gravito-electric tidal tensors, which act as source of the geodesic deviation of nearby test particles, and determine the frame-dragging precession of test gyroscopes. The results of this work can be useful to devise tests of GR through astrophysical observations of close binaries involving a massive BHs and a companion star. Such environments may lead to tidal disruption events

*andrea.maselli@uni-tuebingen.de
†kostas.kokkotas@uni-tuebingen.de
‡plaguna@gatech.edu

even at large distances, producing detectable gravitational and x-ray/UV radiation [27].

In order to test our theoretical framework, we simulate the orbital evolution of BH-white dwarf (WD) binaries, using the new formulation of the gravito-electric tidal tensor together with the affine model, which is a semi-analytical approach to describe star deformations induced by an external quadrupolar tidal field. Originally developed to study the evolution of normal stars or WDs within a Newtonian scheme [28–30], this model was recently improved to describe neutron star tidal disruption events in compact binaries, taking into account relativistic effects on the stellar structure [31,32] and post-Newtonian corrections both on the orbital dynamics and the tidal field [33,34].

With this framework, we follow quasiequilibrium sequences of prototype BH-WD binaries for different modified Kerr metrics, finding that the stellar deformations may vary with respect to the GR case up to 5% even for large distances. For each binary configuration, we also identify the onset of the mass transfer from the star to the companion object, which can be used as initial data for fully relativistic numerical simulations, to investigate the properties of the accreting flow onto the BH.

This paper is organised as follows. In Sec. II, we introduce the JP metric, and we derive the basic features of geodesic motion. In Sec. III, we describe the procedure to characterize the tidal field in the JP space-time, and we explicitly compute the gravito-magnetic and gravito-electric tidal tensors. Moreover, we discuss the relevance of the corrections induced by the strong-gravity modifications of the Kerr metric, comparing our analytical results with those obtained for the pure GR scenario. In Sec. IV, we numerically investigate tidal disruption events in BH-WD binaries, for different configurations. Finally, in Sec. V, we draw the conclusions.

We use Greek letters $(\alpha, \beta, \ldots)$ to denote space-time indices and Latin characters $(i, j, \ldots)$ for spatial indices.

II. JP METRIC

The Johannsen-Psaltis metric is described in Boyer-Lindquist coordinates $x^\mu = (t, r, \theta, \phi)$ by the following line element,

$$\begin{aligned} ds^2 = &-(1+h)\left(1-\frac{2Mr}{\Sigma}\right)dt^2 + \frac{\Sigma(1+h)}{\Delta + a^2\sin^2\theta h}dr^2 \\ &+ \Sigma d\theta^2 - \frac{4aMr\sin^2\theta}{\Sigma}(1+h)dtd\phi \\ &+ \left[r^2 + a^2 + \frac{2a^2Mr\sin^2\theta}{\Sigma} + h\frac{a^2(\Sigma+2Mr)}{\Sigma}\sin^2\theta\right] \\ &\times \sin^2\theta d\phi^2, \end{aligned} \tag{1}$$

where $\Sigma = r^2 + a^2\cos^2\theta$ and $\Delta = r^2 + a^2 - 2Mr$. The function $h(r,\theta)$ parametrizes the deviations from the *pure* Kerr space-time and is given by

$$h(r,\theta) = \sum_{k=0}^{\infty}\left(\epsilon_{2k} + \epsilon_{2k+1}\frac{Mr}{\Sigma}\right)\left(\frac{M^2}{\Sigma}\right)^k. \tag{2}$$

The JP metric has an infinite number of deformations parameters. However, some of them are constrained by theoretical and experimental bounds. As noted in Ref. [26], the requirement $\epsilon_0 = 0$ represents a sufficient condition to guarantee that Eq. (1) satisfies asymptotic flatness at spatial infinity. Moreover, limits on the coefficients $\epsilon_{1,2}$ can be obtained from weak-field tests of gravity within the parametrized post-Newtonian framework, performed in the Solar System [35]. Such bounds translate into $|\epsilon_1| \lesssim 10^{-5}$ and $|\epsilon_2| \lesssim 4.6 \times 10^{-4}$ [15].

In this work, we assume ϵ_3 as the only nonvanishing parameter of $h(r,\theta)$. Such a coefficient is currently unconstrained by observations and reflects changes of the Kerr metric at the order $\sim(M/r)^3$. We also focus on the orbital motion of massive test particles on equatorial circular geodesics, for which $\theta = \pi/2$. This condition further reduces Eq. (2) to

$$h = \epsilon_3\frac{M^3 r}{\Sigma^2} = \epsilon_3\frac{M^3}{r^3}. \tag{3}$$

Finally, we consider the strong-field effects identified by h, as small perturbations of the Kerr geometry, i.e. $\epsilon_3 M^3/r^3 \ll 1$. We develop our framework at the linear approximation, neglecting $\mathcal{O}(h^2)$ corrections. The typical values ϵ_3 considered in literature so far to analyze possible signatures of the JP metric are of the order $\sim\mathcal{O}(10)$ [14,15,20–22,26]. As shown in Fig. 1, for such values, the condition $h \ll 1$ is satisfied whenever the test particle orbits around the black hole at distances greater than $r \sim 6M$. This requirement is consistent with the study of astrophysical systems composed of a supermassive black

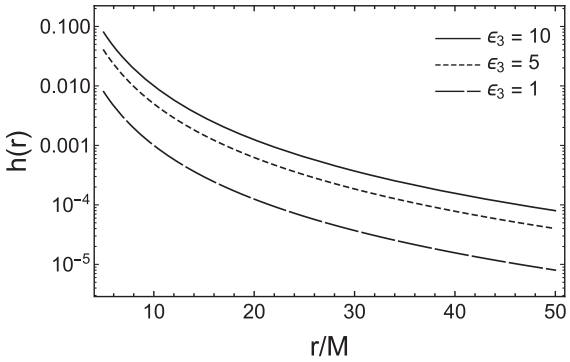

FIG. 1. We show the behavior of $h(r)$ of Eq. (3) as function of the orbital distance normalized to the BH mass, for three values of the parameter $\epsilon_3 = (1, 5, 10)$.

hole and a solar-type star or a white dwarf, which are the primary target of our analysis [36]. It is worth remarking that the parameter ϵ_3 is expected to modify the BH quadrupole moment. This could affect the properties of geodesics around the central objects, varying the nodal precession frequency [37–39] or leading to vertical instabilities in the orbits [40,41].

The JP metric Eq. (1) is characterized by two killing vectors k^μ and m^μ associated to the space-time invariance with respect to time shifts and rotations along the polar angle ϕ. The orbital motion of a test particle with 4-velocity $u^\mu = dx^\mu/d\tau = (u^t, 0, 0, u^\phi)$, τ being the proper time, is then featured by two conserved quantities related to k^μ and m^μ,

$$u^\mu k_\mu = u^t g_{tt} + u^\phi g_{t\phi} = -\mathcal{E}, \tag{4}$$

$$u^\mu m_\mu = u^\phi g_{\phi\phi} + u^t g_{t\phi} = L. \tag{5}$$

which can be identified with the energy at infinity and the angular momentum per unit mass of the test particle, respectively. An analytic expressions for $\mathcal{E}$ and L may be derived solving the system of equations $V_{\rm eff} = 0$ and $V'_{\rm eff} = 0$, where

$$V_{\rm eff}(r) = \frac{1}{g_{rr}}\left[\frac{g_{\phi\phi}\mathcal{E}^2 + 2g_{t\phi}\mathcal{E}L + g_{tt}L^2}{g_{t\phi}^2 - g_{tt}g_{\phi\phi}} - 1\right] \tag{6}$$

is an effective potential governing the geodesic motion of a stationary and axisymmetric space-time [42]. From Eq. (6) and its derivative, we obtain at the linear order in h

$$\mathcal{E} = \frac{1}{N}\left(1 - \frac{2M}{r} + a\omega_{\rm k}\right) - \frac{h}{N^3}\left[\frac{3}{4}\frac{a^2}{r^2} + \frac{1}{4} - ar^2\omega_{\rm k}^3 - \frac{\omega_{\rm k}^2}{2}(r^2 + 6a^2) + \frac{3}{2}\frac{a^3}{r^2}\omega_{\rm k}\right], \tag{7}$$

and

$$L = \frac{r^2\omega_{\rm k}}{N}\left(1 + \frac{a^2}{r^2} - 2a\omega_{\rm k}\right) - \frac{h}{N^3}\left[r^2(a^2 + 3r^2)\omega_{\rm K}^3 + \left(\frac{3a^4}{2r^2} - a^2 - 3r^2\right)\omega_{\rm k} + \frac{3}{4\omega_{\rm k}}\left(1 + \frac{a^2}{r^2}\right) - \left(3a^3 + \frac{9ar^2}{2}\right)\omega_{\rm K}^2 + \frac{9a}{4r^2}(r^2 + a^2)\right], \tag{8}$$

where $\omega_{\rm k} = (M/r^3)^{1/2}$ is the *Keplerian* orbital frequency and we have defined $N = (1 + 2a\omega_{\rm k} - 3r^2\omega_{\rm k}^2)^{1/2}$. Replacing the former expressions into Eqs. (4) and (5) leads to the 4-velocity components u^t and u^ϕ:

$$u^t = \frac{1 + a\omega_{\rm k}}{N} - \frac{h}{N^3 4r^2}[3a^2 + 5r^2 + 6a(a^2 + r^2)\omega_{\rm k} - 4r^2(4a^2 + 3r^2)\omega_{\rm K}^2 + 12ar^4\omega_{\rm k}^3], \tag{9}$$

$$u^\phi = \frac{\omega_{\rm k}}{N} - \frac{h}{4r^2\omega_{\rm k}N^3}[6a^2\omega_{\rm k}^2 + a\omega_{\rm k}(9 - 16r^2\omega_{\rm k}^2) + 3(1 - 2r^2\omega_{\rm k}^2)^2]. \tag{10}$$

III. TIDAL FIELD

In GR, the effects of the stationary gravitational field are described by tidal forces acting on test masses. Single geodesics cannot detect gravity, and at least a pair of them is needed. In the presence of a mass M, the space-time is equipped with a metric $g_{\mu\nu}$, and a test body with 4-velocity u^μ will follow timelike geodesics of this metric. If we assume a second test particle, the position of which with respect to the first one is defined by the displacement vector δx^μ, we can study the relative motion between them using a quasi-inertial Fermi coordinate system [43]. For this purpose, let us consider an orthonormal tetrad[1] $\lambda^\mu{}_{(\alpha)}$ attached to m (which stays forever at the origin of this coordinate frame), parallel transported along its geodesic parametrized by the proper time τ. In Fermi coordinates, the metric at the second order in the displacement vector $y^{(i)} = \lambda^{(i)}{}_\mu \delta x^\mu$ will be given by

$$g_{00} = -1 - R_{(0)(i)(0)(j)}y^{(i)}y^{(j)} + \cdots, \tag{11}$$

$$g_{0i} = -\frac{2}{3}R_{(0)(j)(i)(k)}y^{(j)}y^{(k)} + \cdots, \tag{12}$$

$$g_{ij} = \delta_{ij} - \frac{1}{3}R_{(i)(k)(j)(l)}y^{(k)}y^{(l)} + \cdots, \tag{13}$$

where $R_{(\mu)(\nu)(\rho)(\sigma)}$ is the projection of the Riemann curvature tensor onto the orthonormal tetrad frame

$$R_{(\mu)(\nu)(\rho)(\sigma)} = R_{\alpha\beta\gamma\delta}\lambda^\alpha{}_{(\mu)}\lambda^\beta{}_{(\nu)}\lambda^\gamma{}_{(\rho)}\lambda^\delta{}_{(\sigma)}. \tag{14}$$

From this equation, we can define the *gravito-electric* and *gravito-magnetic* tidal tensors,

$$\mathcal{E}_{(i)(j)} = R_{(0)(i)(0)(j)}, \tag{15}$$

$$\mathcal{H}_{(i)(j)} = -\frac{1}{2}\epsilon_{ikl}R^{(k)(l)}{}_{(0)(j)}, \tag{16}$$

with ϵ_{ijk} being the Levi-Civitá symbol. The electric component $\mathcal{E}_{(i)(j)}$ describes tidal deviations of nearby geodesics, while the magnetic term $\mathcal{H}_{(i)(j)}$ is directly related to frame-dragging effects of test gyroscopes. Both tensors

[1]Hereafter, indices within round brackets will refer to tetrad components.

are symmetric and trace free. This setup is physically equivalent, in the case of negligible Fermi velocity, to solving the geodesic deviation equation, which can be written in the tetrad frame $\lambda^{\mu}{}_{(\alpha)}$ as [44]

$$\frac{d^2 y_{(i)}}{d\tau^2} + \mathcal{E}_{(i)(j)} y^{(j)} = 0. \tag{17}$$

In this section, we shall derive the expressions for Eqs. (15) and (16) in the JP metric, following the approach adopted from Ref. [43]. To determine the parallel transported vectors $\lambda^{\mu}{}_{(\alpha)}$, we first consider the tetrad $e^{\mu}{}_{(\alpha)}$ associated to a static observer in the space-time (1), such that the line element takes the form

$$ds^2 = \eta_{\alpha\beta} d\xi^{(\alpha)} d\xi^{(\beta)}, \tag{18}$$

where $\eta_{\alpha\beta} = \mathrm{diag}(-1, 1, 1, 1)$ is the flat-space metric tensor and $d\xi^{(\alpha)} = e^{(\alpha)}{}_{\mu} dx^{\mu}$. We immediately note from Eq. (1) that for $e^{(1)}{}_{\mu}$ and $e^{(2)}{}_{\mu}$ the basis vectors reduce to

$$e^{(1)}{}_{\mu} = \left(0, \frac{r}{\Delta^{1/2}}\left[1 + \frac{r^2 f h}{2\Delta}\right], 0, 0\right), \tag{19}$$

$$e^{(2)}{}_{\mu} = (0, 0, r, 0). \tag{20}$$

The other two components can be derived from the orthogonality condition $\eta_{\alpha\beta} e^{(\alpha)}{}_{\mu} e^{(\alpha)}{}_{\mu} = g_{\mu\nu}$, from which we find

$$e^{(0)}{}_{\mu} = \left(f[1 + h/2], 0, 0, \frac{2aM}{rf}[1 + h/2]\right), \tag{21}$$

$$e^{(3)}{}_{\mu} = \left(0, 0, 0, \frac{\sqrt{\Delta}}{f} + \frac{a^2 h}{2f\Delta^{1/2}}\right), \tag{22}$$

where $f = \sqrt{1 - 2M/r}$.

The parallel transported tetrad can be now obtained applying to $\lambda^{\mu}{}_{(\alpha)}$ a Lorentz boost along the 3-direction, such that the time component of the new reference frame coincides with the test particle 4-velocity u^{μ}. The new basis vectors on the worldline read

$$\lambda^{\mu}{}_{(0)} = \gamma[e^{\mu}{}_{(0)} + \beta e^{\mu}{}_{(3)}], \qquad \lambda^{\mu}{}_{(1)} = e^{\mu}{}_{(1)}, \tag{23}$$

$$\lambda^{\mu}{}_{(2)} = e^{\mu}{}_{(2)}, \qquad \lambda^{\mu}{}_{(3)} = \gamma[e^{\mu}{}_{(0)} + \beta e^{\mu}{}_{(3)}], \tag{24}$$

where β and γ are the boost velocity and the corresponding Lorentz factor. They can be easily obtained from the condition $\lambda^{\mu}{}_{(0)} = u^{\mu}$, from which we find

$$\gamma = \frac{1}{Nf}[1 + \omega_{\mathrm{k}}(a - 2r^2\omega_{\mathrm{k}})] - \frac{h}{4r^2 N^3 f}[6a^3\omega_{\mathrm{k}} + a^2(3 - 8r^2\omega_{\mathrm{k}}^2) + 2ar^2\omega_{\mathrm{k}}(3 - 5r^2\omega_{\mathrm{k}}^2) + 3r^2(1 - 2r^2\omega_{\mathrm{k}}^2)^2], \tag{25}$$

$$\beta = \frac{\omega_{\mathrm{k}}\Delta^{1/2}}{1 + \omega_{\mathrm{k}}(a - 2r^2\omega_{\mathrm{k}})} - \frac{hf^2}{4\omega_{\mathrm{k}}}\frac{\Delta^{-1/2}}{(r + ar\omega_{\mathrm{k}} - 2M)^2} \times [a^2(3 - 8r^2\omega_{\mathrm{k}}^2) + 2ar^2\omega_{\mathrm{k}}(3 - 5r^2\omega_{\mathrm{k}}^2) + 6a^3\omega_{\mathrm{k}} + 3r^2 f^4]. \tag{26}$$

The time component of the tetrad $\lambda^{\mu}{}_{(0)}$ is automatically parallel transported along the particle wordline, as the vector $\lambda^{\mu}{}_{(2)}$. However, the two spatial vectors $\lambda^{\mu}{}_{(1)}$ and $\lambda^{\mu}{}_{(3)}$, which in spherical polar coordinates are along the radial and tangential directions with respect to the orbit, must to be rotated to be parallel propagated. Therefore, we introduce two new vectors $\tilde{\lambda}^{\mu}{}_{(1)}, \tilde{\lambda}^{\mu}{}_{(3)}$, defined as

$$\tilde{\lambda}^{\mu}{}_{(1)} = \lambda^{\mu}{}_{(1)} \cos\xi - \lambda^{\mu}{}_{(3)} \sin\xi, \tag{27}$$

$$\tilde{\lambda}^{\mu}{}_{(3)} = \lambda^{\mu}{}_{(1)} \sin\xi + \lambda^{\mu}{}_{(3)} \cos\xi. \tag{28}$$

Requiring that $\tilde{\lambda}^{\mu}_{(1)}$ and $\tilde{\lambda}^{\mu}_{(3)}$ satisfy the parallel transport equation along the wordline with tangent vector $\lambda^{\mu}_{(0)}$

$$\lambda^{\nu}{}_{(0)}(\nabla_{\nu}\tilde{\lambda}^{\mu}{}_{(1)}) = \lambda^{\nu}{}_{(0)}(\nabla_{\nu}\tilde{\lambda}^{\mu}{}_{(3)}) = 0, \tag{29}$$

yields for the ξ:

$$\xi = \omega_{\mathrm{k}}\tau\left(1 - \frac{3r - 4M}{4M}h\right), \tag{30}$$

having fixed the integration constant such that $\xi(\tau = 0) = 0$. The full expression for the basis vectors $(\lambda^{\mu}{}_{(0)}, \tilde{\lambda}^{\mu}{}_{(1)}, \lambda^{\mu}{}_{(2)}, \tilde{\lambda}^{\mu}{}_{(3)})$ at the linear order in h is given in the Appendix A.

Having computed the parallel transported tetrad, we can now project the $R_{\alpha\beta\gamma\delta}$ to derive the gravito-electric and gravito-magnetic tensors (15)–(16). For the sake of clarity, we split each component as a sum of two pieces: one related to the pure Kerr geometry and one corresponding to the corrections induced by the parameter h in the JP metric,

$$\mathcal{E}_{(i)(j)} = \bar{\mathcal{E}}_{(i)(j)} + h\delta\mathcal{E}_{(i)(j)}, \tag{31}$$

where

$$\bar{\mathcal{E}}_{(1)(1)} = \omega_{\mathrm{k}}^2\left(1 - \frac{3}{r^2}\frac{\Delta}{N^2}\cos^2\xi\right), \tag{32}$$

$$\bar{\mathcal{E}}_{(2)(2)} = \frac{\omega_{\mathrm{k}}^2}{N^2}\left(1 + 3\frac{a^2}{r^2} - 4a\omega_{\mathrm{k}}\right), \tag{33}$$

$$\bar{\mathcal{E}}_{(3)(3)} = \omega_{\rm k}^2\left(1-\frac{3}{r^2}\frac{\Delta}{N^2}\sin^2\xi\right), \tag{34}$$

$$\bar{\mathcal{E}}_{(1)(3)} = -\frac{3}{2}\frac{\Delta}{N^2 r^2}\omega_{\rm k}^2\sin 2\xi, \tag{35}$$

with $\bar{\mathcal{E}}_{22} = -(\bar{\mathcal{E}}_{11}+\bar{\mathcal{E}}_{33})$ and ξ given by Eq. (30). The changes to the electric tidal tensor induced by the strong field deviations read

$$\begin{aligned}\delta\mathcal{E}_{(1)(1)} =& \frac{4\omega_{\rm k}^2 r^2-3}{2r^2}\sin^2\xi+\frac{1}{2r^4N^4}[3(5a^2+4r^2)\\ &+(51a^3+39ar^2)\omega_{\rm k}+(42a^4-48a^2r^2-80r^4)\omega_{\rm k}^2\\ &-2(66a^3r^2+85ar^4)\omega_{\rm k}^3+(40a^2r^4+183r^6)\omega_{\rm k}^4\\ &+192ar^6\omega_{\rm K}^5-144r^8\omega_{\rm k}^6]\cos^2\xi,\end{aligned} \tag{36}$$

$$\begin{aligned}\delta\mathcal{E}_{(2)(2)} =& \frac{1}{N^4r^2}\left[-\frac{3}{2}\left(3+\frac{5a^2}{r^2}\right)-\frac{3}{2}a\left(9+\frac{17a^2}{r^2}\right)\omega_{\rm k}\right.\\ &+\left(30a^2-\frac{21a^4}{r^2}+29r^2\right)\omega_{\rm K}^2+(66a^3+59ar^2)\omega_{\rm k}^3\\ &\left.-(28a^2r^2+66r^4)\omega_{\rm k}^4-72ar^4\omega_{\rm k}^5+54\omega_{\rm k}^6r^6\right],\end{aligned} \tag{37}$$

$$\begin{aligned}\delta\mathcal{E}_{(3)(3)} =& \frac{4\omega_{\rm k}^2 r^2-3}{2r^2}\cos^2\xi+\frac{1}{2r^4N^4}[3(5a^2+4r^2)\\ &+(51a^3+39ar^2)\omega_{\rm k}+(42a^4-48a^2r^2-80r^4)\omega_{\rm k}^2\\ &-2(66a^3r^2+85ar^4)\omega_{\rm k}^3+(40a^2r^4+183r^6)\omega_{\rm k}^4\\ &+192ar^6\omega_{\rm K}^5-144r^8\omega_{\rm k}^6]\sin^2\xi,\end{aligned} \tag{38}$$

$$\begin{aligned}\delta\mathcal{E}_{(1)(3)} =& \frac{1}{N^4r^4}\left[\frac{15}{4}(a^2+r^2)+\frac{51}{4}a(r^2+a^2)\omega_{\rm k}\right.\\ &+\frac{3}{2}(7a^4-6a^2r^2-17r^4)\omega_{\rm k}^2-\frac{3}{2}(22a^3r^2+37ar^4)\omega_{\rm k}^3\\ &\left.+\left(6a^2r^4+\frac{117}{2}r^6\right)\omega_{\rm k}^4+60ar^6\omega_{\rm k}^5-45r^8\omega_{\rm k}^6\right]\sin 2\xi.\end{aligned} \tag{39}$$

Similarly, the nonvanishing components of the magnetic term (16) are

$$\bar{\mathcal{H}}_{(1)(2)} = -3\frac{\omega_{\rm k}^2}{r^2}(\omega_{\rm k}r^2-a)\frac{\Delta^{1/2}}{N^2}\cos\xi, \tag{40}$$

$$\bar{\mathcal{H}}_{(2)(3)} = -3\frac{\omega_{\rm k}^2}{r^2}(\omega_{\rm k}r^2-a)\frac{\Delta^{1/2}}{N^2}\sin\xi, \tag{41}$$

and finally

$$\begin{aligned}\delta\mathcal{H}_{(1)(2)} =& -\frac{\Delta^{-1/2}}{r^2N^4}\left[\left(33a^2+\frac{18a^4}{r^2}+11r^2\right)\frac{\omega_{\rm k}}{4}\right.\\ &+\left(\frac{27}{2}a^3+\frac{9a^5}{r^2}+2ar^2\right)\omega_{\rm k}^2\\ &-\frac{\omega_{\rm k}^3}{4}(72a^4+163a^2r^2+55r^4)\\ &-\left(18a^3r^2-\frac{ar^4}{2}\right)\omega_{\rm k}^4+(47a^2r^4+21r^6)\omega_{\rm k}^5\\ &\left.-9ar^6\omega_{\rm k}^6-9r^8\omega_{\rm k}^7\right]\cos\xi,\end{aligned} \tag{42}$$

$$\begin{aligned}\delta\mathcal{H}_{(2)(3)} =& -\frac{\Delta^{-1/2}}{r^2N^4}\left[\left(45a^2+\frac{18a^4}{r^2}+27r^2\right)\frac{\omega_{\rm k}}{4}\right.\\ &+\left(\frac{51a^3}{2}+\frac{9a^5}{r^2}+15ar^2\right)\omega_{\rm k}^2\\ &-(24a^4+195a^2r^2+171r^4)\frac{\omega_{\rm k}^3}{4}\\ &-\left(54a^3r^2+\frac{117ar^4}{2}\right)\omega_{\rm k}^4+(54a^2r^4+90r^6)\omega_{\rm k}^5\\ &\left.+57ar^6\omega_{\rm k}^6-63r^8\omega_{\rm k}^7\right]\sin\xi.\end{aligned} \tag{43}$$

A. Relevance of strong-gravity corrections

Given the explicit form of the gravito-magnetic and electric tidal tensors, Eqs. (32)–(43), we need to estimate the relevance of the non-Kerr components as function of the BH angular momentum and the deformation parameter ϵ_3. To this aim, we define the two quantities

$$\Delta\mathcal{E}_{ij} = h\frac{\delta\mathcal{E}_{(i)(j)}}{\bar{\mathcal{E}}_{(i)(j)}} \quad \text{and} \quad \Delta\mathcal{H}_{ij} = h\frac{\delta\mathcal{H}_{(i)(j)}}{\bar{\mathcal{H}}_{(i)(j)}}, \tag{44}$$

which represent the fractional change with respect to $\mathcal{E}$ and $\mathcal{H}$ computed in the standard GR scenario. In the following, starting from an initial configuration with $\xi(\tau_0)=0$, we consider snapshots at different orbital distances with the same phase $\xi(\tau)=\xi(\tau_0)$. Even though a more accurate analysis will be developed in the next section through a numerical approach, this assumption will provide, as first hint, an order of magnitude estimate of the effects we are going to study. We note that in this case $\mathcal{E}_{(1)(3)}=\mathcal{H}_{(2)(3)}=0$. Our results can be summarized in Figs. 2–4.

In the three panels of Fig. 2, we show the absolute value of $\Delta\mathcal{E}_{ij}$ as a function of the orbital distance, for $\epsilon_3=(1,5,10)$ and BH spin parameter $a/M=0.5$. As expected, the contribution of strong-gravity terms grows as r decreases and can be of the order $\sim 10\%$ for $r>10M$. For $r<6M$ and $\epsilon_3>5$, the relative difference is always

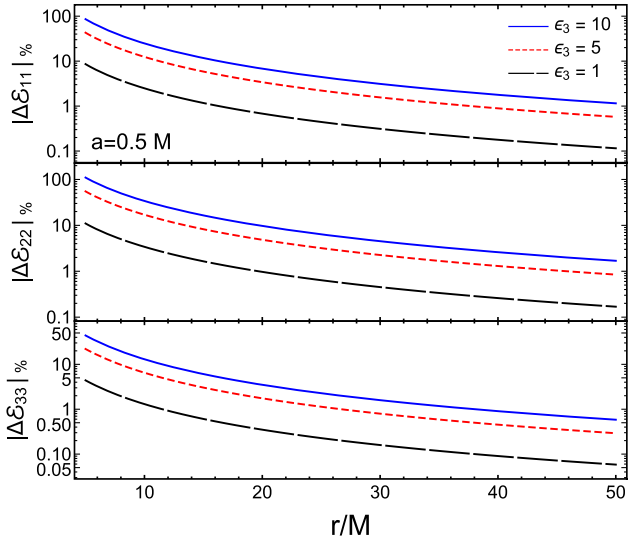

FIG. 2. In this figure, we plot the absolute percentage values of $\Delta\mathcal{E}_{ij}$ given by Eq. (44) as a function of the orbital distance, for three values of the strong-gravity parameter $\epsilon_3 = (1, 5, 10)$, and BH spin $a = 0.5M$.

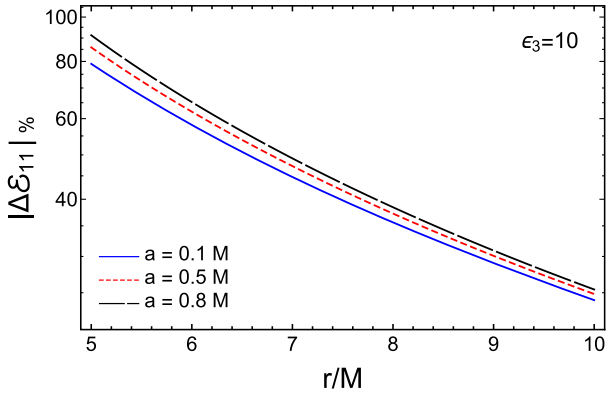

FIG. 3. Same as Fig. 2 but only for $\Delta\mathcal{E}_{11}$, with $\epsilon_3 = 10$ and different values of the BH spin parameter $a/M = (0.1, 0.5, 0.8)$.

larger than 50%; terms of second order $\mathcal{O}(h^2)$ and proportional to higher coefficients as ϵ_4 start to be relevant and cannot be neglected. For $\epsilon_3 > 0$ (< 0 respectively), all the components of $\Delta\mathcal{E}_{ij}$ are smaller (higher) than zero, and therefore the strong-gravity corrections reduce (increase) the neat effect of tidal deviations induced by the gravito-electric tensor.[2]

In Fig. 3, we draw $\Delta\mathcal{E}_{11}$ for $\epsilon_3 = 10$ and different values of $a/M = (0.1, 0.5, 0.8)$. The plot shows that, unless the binary systems gets very close at orbital distances $r \ll 10M$, the effects of non-Kerr deviations seem to be

[2]This feature could be qualitatively expected since for $\epsilon_3 > 0$ ($\epsilon_3 < 0$) the modified BH is more prolate (oblate) than the Kerr one [20].

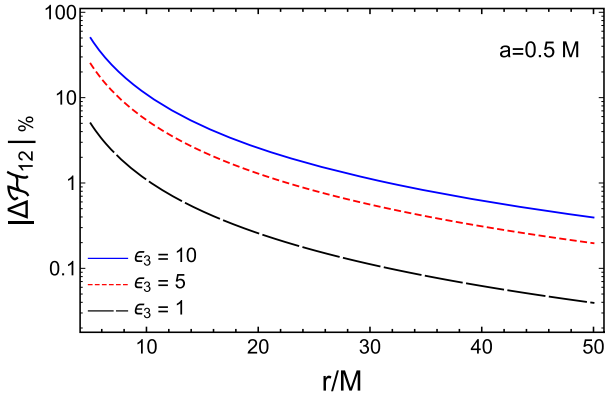

FIG. 4. Same as Fig. 2 but for the magnetic component $\Delta\mathcal{H}_{12}$.

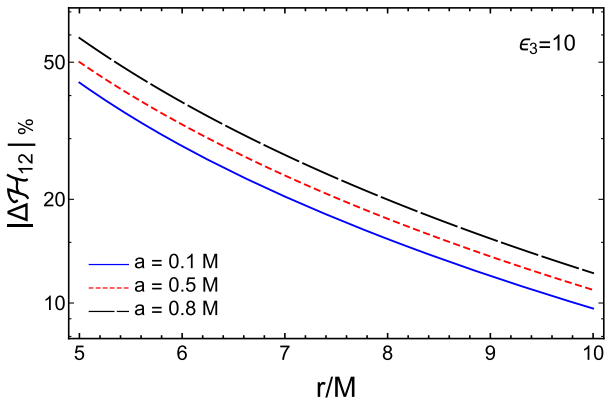

FIG. 5. Same as Fig. 3 but for the magnetic component $\Delta\mathcal{H}_{12}$.

insensitive to the BH spin. This feature does not change for the other components of $\mathcal{E}_{(i)(j)}$.

Finally, we note that the picture described above also applies to the gravito-magnetic tidal tensor. We show the behavior of $\Delta\mathcal{H}_{12}$ in Figs. 4 and 5 for the same set of parameters previously considered.

IV. BLACK HOLE-WHITE DWARF BINARY EVOLUTION

Hereafter, we will analyze the effects of strong-field corrections derived in the previous section, using our results together with the affine model, which represents a semianalytic approach to describing stellar deformations induced by an external tidal field. We shall first provide a brief summary of the main ingredients of the model, referring the reader to Ref. [34] (and references therein) for a more comprehensive description of this framework. Then, we will present the numerical results obtained for different configurations of prototype BH-WD binaries.

A. Model

The main assumption of the affine approach is that the spherical star is deformed by the tidal field into an ellipsoid,

preserving this shape during the orbital motion. More specifically, it is warped in an S-type Riemann ellipsoid, for which the spin and vorticity are parallel and their ratio constant [45]. The equations for the stellar deformations are written in the *principal frame*, which is comoving with the star, and such that the axes are adapted to the principal axes of the ellipsoid[3] $a_{i=1,2,3}$. Under this assumption, the infinite number of degrees of freedom of the internal fluid is reduced to a set of five variables $(a_1, a_2, a_3, \psi, \lambda)$, where ψ and λ are the two angles:

$$\frac{d\psi}{d\tau} = \Omega, \qquad \frac{d\lambda}{d\tau} = \Lambda. \tag{45}$$

In the previous expressions, Ω is the WD angular velocity measured in the tetrad coordinate system (which is parallel transported), and Λ describes the internal fluid motion in the principal frame.

The equations of motion for the star can be derived from the Lagrangian

$$\mathcal{L} = \mathcal{L}_{\rm B} + \mathcal{L}_{\rm T}, \tag{46}$$

where the subscripts T and B refer to *tidal* and *body*. The first term reads

$$\mathcal{L}_{\rm T} = -\frac{1}{2} c_{ij} I_{ij}, \tag{47}$$

where I_{ij}s the inertial tensor, which is written in the affine model as

$$I_{ij} = \hat{\mathcal{M}} \cdot \mathrm{diag}\left(\frac{a_i}{R_{\rm WD}}\right)^2 = \frac{4\pi}{3}\int_0^{R_{\rm WD}} \hat{\rho}(r) r^4 dr, \tag{48}$$

$\hat{\mathcal{M}}$ being the scalar quadrupole moment computed over the density profile of the star[4] and $R_{\rm WD}$ its radius at spherical equilibrium. c_{ij} are the components of the gravito-electric tidal tensor in the principal frame, obtained by rotating $\mathcal{E}_{ij}$ of the angle ψ [defined in Eq. (45)] $c = T\mathcal{E}T^T$, where the matrix T is given by

$$T = \begin{pmatrix} \cos\psi & 0 & \sin\psi \\ 0 & 1 & 0 \\ -\sin\psi & 0 & \cos\psi \end{pmatrix}. \tag{49}$$

Practically speaking, this rotation changes the angle ξ into $l = \psi - \xi$. The latter describes the misalignment between the a_1 axis and the line between the two objects: when l is negligible, the binary is said to be *synchronized*. For a star with zero viscosity, this angle is in general very small. However, as the orbit shrinks, the tidal bulge lags behind the tidal potential and then is subject to a torque which tries to spin it to follow the orbital motion, and the system desynchronizes [46,47].

The body Lagrangian $\mathcal{L}_{\rm B}$ describes the star internal dynamics and contains three contributions coming from the kinetic, the internal energy of the fluid, and the self-gravity (see Ref. [34] for a complete expression of these quantities in terms of the affine model variables). By applying the Euler-Lagrange formalism to Eq. (46), we obtain the equations of motion for the star,

$$\ddot{a}_1 = a_1(\Lambda^2 + \Omega^2) - 2a_2\Lambda\Omega + \frac{1}{2}\frac{\hat{V}}{\hat{\mathcal{M}}} R_{\rm WD}^3 a_1 A_1 - \frac{R_{\rm WD}^2}{\mathcal{M}}\frac{\hat{V}}{3a_1} - c_{11}a_1, \tag{50}$$

$$\ddot{a}_3 = a_3(\Lambda^2 + \Omega^2) - 2a_1\Lambda\Omega + \frac{1}{2}\frac{\hat{V}}{\hat{\mathcal{M}}} R_{\rm WD}^3 a_3 A_3 - \frac{R_{\rm WD}^2}{\hat{\mathcal{M}}}\frac{\hat{V}}{3a_3} - c_{33}a_3, \tag{51}$$

$$\ddot{a}_2 = \frac{1}{2}\frac{\hat{V}}{\hat{\mathcal{M}}} R_{\rm WD}^3 a_2 A_2 - \frac{R_{\rm WD}^2}{\hat{\mathcal{M}}}\frac{\hat{V}}{3a_2} - c_{22}a_2, \tag{52}$$

$$\dot{J} = \frac{\hat{\mathcal{M}}}{R_{\rm WD}^2} c_{13}(a_3^2 - a_1^2), \tag{53}$$

$$\dot{\mathcal{C}} = 0, \tag{54}$$

where a dot refers to differentiation with respect to the proper time τ and $\hat{V}$ is the star self-gravity at spherical equilibrium, given by

$$\hat{V} = -\frac{G}{2}\int_{\rm spher} r\partial_r \Phi_{\rm Newt} dm, \tag{55}$$

with $\Phi_{\rm Newt}$ the Newtonian gravitational potential and dm the WD mass element. We have also introduced the quantities

$$A_i = \int_0^\infty \frac{du}{(a_i^2 + u)\sqrt{(a_1^2 + u)(a_2^2 + u)(a_3^2 + u)}}, \tag{56}$$

$$J = \frac{\hat{\mathcal{M}}}{R_{\rm WD}^2}[(a_1^2 + a_3^2)\Omega - 2a_1 a_3 \Lambda], \tag{57}$$

$$\mathcal{C} = \frac{\hat{\mathcal{M}}}{R_{\rm WD}^2}[(a_1^2 + a_3^2)\Lambda - 2a_1 a_3 \Omega], \tag{58}$$

J being the star angular momentum and $\mathcal{C}$ the circulation of the fluid [30]. In the absence of viscosity, as for the models

[3] In the following, "1" denotes the direction along the axis parallel to the orbital separation, "2" identifies the axis orthogonal to the orbital plane, and "3" defines the other axis in the orbital plane.

[4] The superscript hat denotes quantities computed for the spherical star.

we are going to study here, $\mathcal{C}$ is a constant of motion. We also consider irrotational configurations, for which $\mathcal{C}=0$.

In this work, we investigate quasiequilibrium sequences of BH-WD binaries; this assumption reduces Eqs. (50)–(54) to a system of coupled algebraic equations,

$$\ddot{a}_i = 0, \qquad \psi = \xi, \qquad \dot{\psi} = \Omega = \dot{\xi}, \tag{59}$$

which is solved through a Newton-Raphson method.

B. Numerical results

We employ the affine model for a representative set of binary configurations. The WD equilibrium structure is built within a Newtonian framework using a polytropic equation of state $P = K\rho^{\gamma}$ with $\gamma = 5/3$, where P and ρ are the pressure and mass-density profiles. We choose the central density and the constant K such that the star has mass and radius $M_{\rm WD} = 1M_{\odot}$ and $R_{\rm WD} = 7088$ km. Moreover, we consider rotating BHs with mass $M = 10^4 M_{\odot}$, spins $a = (0.5, 0.8)M$, and five values for the deformation parameter of the JP metric $\epsilon_3 = (0, \pm 5, \pm 10)$. For each configuration, we solve the system of Eqs. (59) placing the spherical star at the orbital separation $r \gg R_{\rm WD}$ from the BH. Then, we gradually reduce the distance until it reaches the critical point $r_{\rm tide}$ at which the WD fills its Roche lobe. The latter defines the region around the star in which a particle with mass $m \ll M_{\rm WD}$ is gravitationally bounded to the central object. At the Newtonian level, the Roche lobe can be identified by finding the maximum of the three-body potential (in the equatorial plane x–y),

$$U(x,y) = -\frac{Gm_1}{|\vec{x}-\vec{y}_1|} - \frac{Gm_1}{|\vec{x}-\vec{y}_2|} - \frac{G}{2}\frac{(m_1+m_2)}{|\vec{y}_1-\vec{y}_2|^3}x^2, \tag{60}$$

where $\vec{y}_{1/2}$ are the displacement vectors and in our case $m_1 = M$, $m_2 = M_{\rm WD}$. At each step of the simulation, we numerically compute Eq. (60) and its maximum, defining $r_{\rm tide}$ as the orbital distance for which the WD axis a_1, elongated by the tidal forces, touches the Roche lobe.

Our results can be summarized as follows:

(i) In Fig. 6, we show the relative difference between the axes a_1, a_2 computed for $\epsilon_3 = (\pm 5, \pm 10)$ and $\epsilon_3 = 0$, namely,

$$\Delta a_1 = \frac{a_1|_{\epsilon_3=\pm 5}}{a_1|_{\epsilon_3=0}} - 1, \quad \Delta a_1 = \frac{a_1|_{\epsilon_3=\pm 10}}{a_1|_{\epsilon_3=0}} - 1, \tag{61}$$

as function of the orbital distance normalized to the BH mass, for $a/M = 0.5$. This quantity is evaluated up to the radius[5] $r_{\rm tide}|_{\epsilon_3=0}$ or $r_{\rm tide}|_{\epsilon_3=-5,-10}$, for positive and negative values of ϵ_3, respectively. As the relative separation shrinks, the difference between the GR and the alternative scenario increases up to ∼3% and ∼5% for $\epsilon_3 = \pm 5$ and $\epsilon_3 = \pm 10$, respectively. The effect on the axis a_2 is less pronounced with discrepancies smaller than 1%; the same results apply to the axis a_3.

(ii) In Table I, we show, for each binary configuration considered, the critical distances at which the WD fills its Roche lobe and the related values of the axes normalized to the star radius at spherical equilibrium, $\bar{a}_i = a_i/R_{\rm WD}$. We note that all the simulations end around $r_{\rm tide} \sim 20M_{\rm tot}$. This can be explained looking at the behavior of the gravito-electric tidal tensor in Fig. 1, which shows that the effect of the deformation parameter ϵ_3 plays a crucial role only for distances $r \sim 10M_{\rm tot}$. Finally, as pointed out in the previous section, values of ϵ_3 smaller than zero

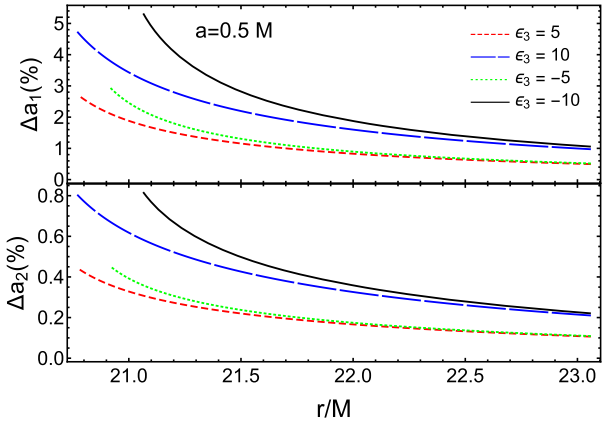

FIG. 6. We show the difference, Eq. (61), between the axes computed for $\epsilon_3 = (\pm 5, \pm 10)$ and $\epsilon_3 = 0$, for $a/M = 0.5$, as a function of the orbital distance divided by the total mass of the system.

TABLE I. For each binary configuration considered, identified by the BH spin a/M and the deformation parameter ϵ_3, we show the critical orbital distance at which the simulation ends and the maximum deformation of the WD axes normalized to its radius at spherical equilibrium $\bar{a}_i = a_i/R_{\rm WD}$.

a	ϵ_3	$r_{\rm tide}/M$	$\bar{a}_1$	$\bar{a}_2$	$\bar{a}_3$
0.5	0	20.773	1.306	0.919	0.947
0.5	5	20.621	1.296	0.919	0.948
0.5	10	20.464	1.287	0.920	0.949
0.5	−5	20.922	1.315	0.919	0.946
0.5	−10	21.066	1.323	0.919	0.945
0.8	0	20.738	1.303	0.919	0.947
0.8	5	20.584	1.294	0.919	0.949
0.8	10	20.426	1.285	0.919	0.950
0.8	−5	20.888	1.312	0.919	0.946
0.8	−10	21.033	1.321	0.918	0.945

[5]As noted in Sec. III A, values of the parameter ϵ_3 greater than zero reduce the effect of the tidal field and then make the star fill its Roche lobe at smaller orbital distances than the pure GR case for which $\epsilon_3 = 0$. Vice versa, for $\epsilon_3 < 0$, the star touches the Roche lobe surface earlier.

increase the strength of the tidal field and make the star fill its Roche lobe at larger distances.

It is worth remarking that the orbital radius $r_{\rm tide}$ does not identify the WD tidal disruption but the distance at which the star begins to lose mass toward the companion object. We expect therefore that the orbital evolution after this critical point, and the dynamics of the accreting flow, will be significantly affected by the Kerr metric modifications. However, such effects can be tracked only by means of numerical codes. This will be the subject of further investigations, in which we will implement the theoretical results developed in the previous section into fully relativistic numerical simulations.

(iii) We have followed the same procedure described above for $a/M = 0.8$, finding again differences at the most of $\Delta a_1 \sim 5\%$ for $\epsilon_3 = \pm 10$. As already noted therefore, the effect of the BH spin does not change the evolutionary picture. This can be easily understood looking at Eqs. (32)–(35): even in the standard Kerr case, the spin starts to provide a significant contribution only for distances $r < 10M$.

V. CONCLUSIONS

Current and future observations in the electromagnetic and gravitational spectrum will allow us to map the space-time around supermassive BHs and to study the properties of the strong gravitational field in their surroundings. In particular, these experiments will shed new light on the validity of the no-hair theorem, for which astrophysical BHs in General Relativity belong to the Kerr family, and are described only by their mass and spin. In this scenario, the quest for model-independent tests of gravity which make use of the incoming flood of data is more needed than ever. Several efforts have been devoted to pursuing this goal. Among the model proposed in literature, we have considered the JP metric, which parametrizes the deviations from the Kerr geometry through a set of free parameters, to be constrained by experiments.

In this work, we focused our attention on the description of tidal effects produced by rotating BHs. We computed the analytic expression for the gravito-magnetic and gravito-electric tidal tensors, which completely describe the quadrupolar nature of the tidal field. We consider the case of equatorial geodesics, expanding all quantities at the linear order in the parameter ϵ_3 (or equivalently h), which identifies the deviations from the Kerr metric. Comparing our results with those obtained in the pure GR case, we have found discrepancies both for $\mathcal{E}$ and $\mathcal{H}$ which can be as high as $\sim 10\%$ even for large distances, $r > 10M$. These differences seem also to weakly depend on the BH angular momentum.

We have implemented our results into a semianalytic approach, called the affine model, to simulate the encounter of BH-WD systems, following the orbital evolution until the star fill its Roche lobe. Analyzing a representative set of binary configurations, we have found that the tidal deformations of the WD can be up to 5% different between the pure GR and the alternative scenario, for $\epsilon_3 = \pm 10$, even at orbital separation $r \sim 20M$. Therefore, we expect that the matter flow onto the BH, and the possible formation of an accreting disk, would be significantly affected by the strong-field correction induced by the JP metric.

Assessing the features and the detectability of such processes will be a matter of future investigations, in which we will implement our theoretical results into fully relativistic numerical simulations.

ACKNOWLEDGMENTS

It is a pleasure to thank Cosimo Bambi for having carefully read the manuscript and for his useful comments. P. L. is supported by the NSF Grants No. 1505824 and No. 1333360.

APPENDIX: THE PARALLEL TRANSPORTED TETRAD IN THE JP SPACE-TIME

In this section, we show the form of the basis vectors $\lambda^{\mu}{}_{(\alpha)}$ parallel propagated along a circular geodesic in the JP space-time, at the linear order in the parameter $h = \epsilon_3 M^3/r^3$,

$$\lambda^{0}{}_{(0)} = \frac{1+a\omega_{\rm k}}{N} - \frac{h}{N^3 4r^2}[3a^2+5r^2+6a(a^2+r^2)\omega_{\rm k} - 4r^2(4a^2+3r^2)\omega_{\rm K}^2 + 12ar^4\omega_{\rm k}^3], \tag{A1a}$$

$$\lambda^{1}{}_{(0)} = 0, \tag{A1b}$$

$$\lambda^{2}{}_{(0)} = 0, \tag{A1c}$$

$$\lambda^{3}{}_{(0)} = \frac{\omega_{\rm k}}{N} - \frac{h}{4r^2\omega_{\rm k}N^3}[6a^2\omega_{\rm k}^2 + a\omega_{\rm k}(9-16r^2\omega_{\rm k}^2) + 3(1-2r^2\omega_{\rm k}^2)^2], \tag{A1d}$$

$$\tilde{\lambda}^{0}{}_{(1)} = -\frac{\sqrt{\Delta}\omega_{\rm k}}{N}\sin\xi + \frac{h\Delta^{-3/2}}{4r^2N^3\omega_{\rm k}}[(a^2+r^2)^2(3+9a\omega_{\rm k}) + 2(a^2+r^2)\omega_{\rm k}^2(3a^4-8r^4) - 4ar^2\omega_{\rm k}^3(a^4+11a^2r^2+9r^4) + 2r^4(13r^4-3a^2r^2-18a^4)\omega_{\rm k}^4 + 8ar^6(5a^2+6r^2)\omega_{\rm k}^5 + 4r^8(5a^2-3r^2)\omega_{\rm k}^6 - 24ar^{10}\omega_{\rm k}^7]\sin\xi, \tag{A2a}$$

$$\tilde{\lambda}^{1}{}_{(1)} = \frac{\Delta^{1/2}}{r}\cos\xi - \frac{h}{2\Delta^{1/2}}(r-2M)\cos\xi, \tag{A2b}$$

$$\tilde{\lambda}^{\tilde{\lambda}}{}_{(1)} = 0, \tag{A2c}$$

$$\tilde{\lambda}^{3}{}_{(1)} = -\frac{1+\omega_{\rm k}(a-2r^2\omega_{\rm k})}{N\Delta^{1/2}}\sin\xi + \frac{h}{4r^2N^3\Delta^{3/2}}[6a^5\omega_{\rm k} + a^4(3-4r^2\omega_{\rm k}^2) + 18a^3r\omega_{\rm k}(r-2M) + 3r(r-2M)^3 + 4a^2r^2(2-9r^2\omega_{\rm k}^2+10r^4\omega_{\rm k}^4) + a(6r^4\omega_{\rm k} - 22r^6\omega_{\rm k}^3 + 20r^8\omega_{\rm k}^5)]\sin\xi, \tag{A2d}$$

$$\lambda^{\lambda}{}_{(2)} = 0, \tag{A3a}$$

$$\lambda^{1}{}_{(2)} = 0, \tag{A3b}$$

$$\lambda^{3}{}_{(2)} = 0, \tag{A3c}$$

$$\lambda^{2}{}_{(2)} = \frac{1}{r}, \tag{A3d}$$

$$\tilde{\lambda}^{0}{}_{(3)} = \frac{\sqrt{\Delta}\omega_{\rm k}}{N}\cos\xi - \frac{h\Delta^{-3/2}}{4r^2N^3\omega_{\rm k}}[(a^2+r^2)^2(3+9a\omega_{\rm k}) + 2(a^2+r^2)\omega_{\rm k}^2(3a^4-8r^4) - 4ar^2\omega_{\rm k}^3(a^4+11a^2r^2+9r^4) + 2r^4(13r^4-3a^2r^2-18a^4)\omega_{\rm k}^4 + 8ar^6(5a^2+6r^2)\omega_{\rm k}^5 + 4r^8(5a^2-3r^2)\omega_{\rm k}^6 - 24ar^{10}\omega_{\rm k}^7]\cos\xi, \tag{A4a}$$

$$\tilde{\lambda}^{1}{}_{(3)} = -\frac{\Delta^{1/2}}{r}\sin\xi - \frac{h}{2\Delta^{1/2}}(r-2M)\sin\xi, \tag{A4b}$$

$$\tilde{\lambda}^{2}{}_{(3)} = 0, \tag{A4c}$$

$$\tilde{\lambda}^{3}{}_{(3)} = \frac{1+\omega_{\rm k}(a-2r^2\omega_{\rm k})}{N\Delta^{1/2}}\cos\xi - \frac{h}{4r^2N^3\Delta^{3/2}}[6a^5\omega_{\rm k} + a^4(3-4r^2\omega_{\rm k}^2) + 18a^3r\omega_{\rm k}(r-2M) + 3r(r-2M)^3 + 4a^2r^2(2-9r^2\omega_{\rm k}^2+10r^4\omega_{\rm k}^4) + a(6r^4\omega_{\rm k} - 22r^6\omega_{\rm k}^3 + 20r^8\omega_{\rm k}^5)]\cos\xi. \tag{A4d}$$

[1] C. M. Will, Living Rev. Relativity **17**, 4 (2014).
[2] E. Berti *et al.*, Classical Quantum Gravity **32**, 243001 (2015).
[3] N. Yunes and X. Siemens, Living Rev. Relativity **16**, 9 (2013).
[4] D. Psaltis, Living Rev. Relativity **11**, 9 (2008).
[5] C. Bambi, arXiv:1509.03884.
[6] D. L. Wiltshire, M. Visser, and S. M. Scott, *The Kerr Spacetime: Rotating Black Holes in General Relativity* (Cambridge University Press, Cambridge, England, 2009).
[7] R. H. Price, Phys. Rev. D **5**, 2419 (1972).
[8] A. E. Broderick, T. Johannsen, A. Loeb, and D. Psaltis, Astrophys. J. **784**, 7 (2014).
[9] F. Eisenhauer *et al.*, Proc. SPIE Int. Soc. Opt. Eng. **7013**, 2A (2008).
[10] M. Feroci *et al.*, Exp. Astron. **34**, 415 (2012).
[11] K. C. Gendreau, Z. Arzoumanian, and T. Okajima, in *Society of Photo-Optical Instrumentation Engineers (SPIE) Conference Series* (2012), Vol. 8443 of Society of Photo-Optical Instrumentation Engineers (SPIE) Conference Series, p. 13.
[12] G. M. Harry and the LIGO Scientific Collaboration, Classical Quantum Gravity **27**, 084006 (2010).
[13] F. Acernese *et al.*, Classical Quantum Gravity **25**, 114045 (2008).
[14] T. Johannsen, Phys. Rev. D **87**, 124017 (2013).
[15] T. Johannsen and D. Psaltis, Phys. Rev. D **83**, 124015 (2011).
[16] E. T. Newman and A. I. Janis, J. Math. Phys. (N.Y.) **6**, 915 (1965).
[17] T. Johannsen and D. Psaltis, Astrophys. J. **716**, 187 (2010).
[18] C. Bambi and L. Modesto, Phys. Lett. B **706**, 13 (2011).

[19] C. Bambi, Phys. Rev. D **85**, 043002 (2012).
[20] C. Bambi, Phys. Lett. B **705**, 5 (2011).
[21] T. Johannsen, Phys. Rev. D **87**, 124010 (2013).
[22] C. Bambi, J. Cosmol. Astropart. Phys. 09 (2012) 014.
[23] C. Bambi, Phys. Rev. D **87**, 023007 (2013).
[24] T. Johannsen and D. Psaltis, Astrophys. J. **773**, 57 (2013).
[25] C. Bambi, Astrophys. J. **761**, 174 (2012).
[26] V. Cardoso, P. Pani, and J. a. Rico, Phys. Rev. D **89**, 064007 (2014).
[27] S. Kobayashi, P. Laguna, E. S. Phinney, and P. Mészáros, Astrophys. J. **615**, 855 (2004).
[28] J.-P. Luminet and J.-A. Marck, Mon. Not. R. Astron. Soc. **212**, 57 (1985).
[29] B. Carter and J. P. Luminet, Mon. Not. R. Astron. Soc. **212**, 23 (1985).
[30] P. Wiggins and D. Lai, Astrophys. J. **532**, 530 (2000).
[31] V. Ferrari, L. Gualtieri, and F. Pannarale, Classical Quantum Gravity **26**, 125004 (2009).
[32] V. Ferrari, L. Gualtieri, and F. Pannarale, Phys. Rev. D **81**, 064026 (2010).
[33] V. Ferrari, L. Gualtieri, and A. Maselli, Phys. Rev. D **85**, 044045 (2012).
[34] A. Maselli, L. Gualtieri, F. Pannarale, and V. Ferrari, Phys. Rev. D **86**, 044032 (2012).
[35] C. M. Will, Living Rev. Relativity **9** (2006).
[36] C. Evans, P. Laguna, and M. Eracleous, Astrophys. J. **805**, L19 (2015).
[37] G. Pappas, Mon. Not. R. Astron. Soc. **422**, 2581 (2012).
[38] G. Pappas, Mon. Not. R. Astron. Soc. **454**, 4066 (2015).
[39] D. Gondek-Rosinska, W. Kluzniak, N. Stergioulas, and M. Wisniewicz, Phys. Rev. D **89**, 104001 (2014).
[40] C. Bambi and E. Barausse, Astrophys. J. **731**, 121 (2011).
[41] J. R. Gair, C. Li, and I. Mandel, Phys. Rev. D **77**, 024035 (2008).
[42] C. Misner, K. Thorne, and J. Wheeler, *Gravitation* (Freeman, San Francisco, 1973).
[43] C. Chicone and B. Mashhoon, Classical Quantum Gravity **23**, 4021 (2006).
[44] F. A. E. Pirani, Acta Phys. Pol. **15**, 389 (1956).
[45] S. S. Chandrasekhar, *Ellipsoidal Figures of Equilibrium* (Yale University, New Haven, CT, 1969), p. 243.
[46] D. Lai, F. A. Rasio, and S. L. Shapiro, Astrophys. J. **423**, 344 (1994).
[47] S. Dall'Osso and E. M. Rossi, Mon. Not. R. Astron. Soc. **428**, 518 (2013).